NATURAL CONVECTION HEAT TRANSFER AND FLUID FLOW IN A THERMAL CHIMNEY WITH MULTIPLE HORIZONTALLY-ALIGHNED CYLINDERS

Haiteng Ma[1,*], L. He[2], Guopeng Yu[3], Zhibin Yu[4]

1. Shanghai Jiao Tong University, Shanghai, China
2. University of Oxford, Oxford, UK
3. Sun Yat-Sen University, Guangdong, China
4. University of Glasgow, Glasgow, UK

ABSTRACT

To address the scarcity of natural convection research for the tube array with three or more columns of horizontally-aligned cylinders, this paper conducts RANS/URANS simulations for multiple cylinder columns in one or two rows, validated by particle-image velocimetry and heat transfer measurements. Parametric study with varying horizontal and vertical pitches is implemented by RANS with transition SST model. Key findings are then substantiated and examined by URANS. It is found that the horizontal pitch influences the balance between the chimney effect and the blockage effect, thus has an optimum with respect to the natural draft velocity. For all the vertical distances computed in the two-row thermal chimney model, the flow pattern stays in a plume-dominant mode at the large horizontal pitch and a chimney-dominant mode at the small horizontal pitch. Interestingly, at the intermediate horizontal pitch (pitch/diameter≈2.5), the flow pattern switches from plume-dominant to chimney-dominant over a minor increase of the vertical pitch (from 4.5 to 6 diameters), leading to significant augmentation in natural draft velocity and heat transfer on cylinder surfaces. This distinct thermo-flow behavior, identified for the first time to the authors' knowledge, may be harnessed to improve the performance of passive heat exchangers.

Key Words:

Natural convection heat transfer, buoyant plume, air-cooled condenser, computational fluid dynamics, thermal chimney

1. INTRODUCTION

Cooling system plays a substantial role in power plants due to its influence on the efficiency and output of power generation thermodynamic cycle. Dry cooling technology, albeit less efficient than wet cooling, has been employed overwhelmingly in arid regions of the world such as southwestern United States and Australian hinterland due to water shortage and environmental concerns (Hooman [1]). Its application is also expected to grow as the water-scarce countries in Africa ramp up power generation capacity for economic development.

Air cooled condenser, as the core component in dry cooling, is traditionally driven by mechanical fans or pumps to enhance heat transfer on its outer surfaces, but this leads to parasitic power loss, noise and higher maintenance cost. Malfunction associated with active cooling devices is also intolerable, particularly for nuclear power plant. For instance, the accident of Fukushima nuclear power plant in 2011 was caused by the failure of cooling devices due to power shut-down during the earthquake.

As an alternative, natural draft air cooled condensers solve these issues and are widely applied in nuclear, coal-fired and geothermal power plants. Ambient air is drawn upward by condenser tubes due to buoyancy or density difference, and cools the condenser accordingly. This kind of passive cooling technology is adopted in the third generation pressurized water reactor (Lai et al. [2]) and the fourth generation molten salt reactor (Zhao et al. [3] and Wu et al. [4]) to enhance inherent safety of the nuclear power plant. Besides, it is extensively deployed in natural draft dry cooling tower to eliminate parasitic loss and save the operational cost in coal-fired (Kröger [5]) and geothermal (Hooman [6]) power plants. A lot of studies were reported on the crosswind effect due to its huge influence on thermo-flow performance of natural draft dry cooling tower (Hooman [1], Lu et al. [7], Kong et al. [8]).

The prime challenge for natural draft air cooled condenser is its cooling capacity is greatly limited by the low heat transfer coefficient on the outer surface of condenser tubes. This is because the draft velocity induced by free convection is usually very small. Experiments on a lab-scale natural draft dry cooling tower reported an upward velocity of 0.54 m/s by Tanimizu and Hooman [9] and 0.32 m/s by Lu et al. [7] near the tower exit. To augment thermal chimney effect which provides the airlift, concept of solar enhanced natural draft dry cooling tower is introduced recently (Zou et al. [10]). Solar collectors are added to traditional natural draft dry cooling towers to increase the suction of ambient air through the compact heat exchangers. Thermal efficiency is also demonstrated to increase for geothermal (Zou et al. [11]) and coal-fired power plant (Ghorbani et al. [12]) with solar chimney integrated. Nevertheless, more measures are needed to enhance natural draft intensity because thermo-flow field is inherently weak and unstable in natural convection, compare to that in forced convection.

As such, a new concept of thermal chimney driven air cooled condenser is proposed, which utilizes waste heat to strengthen the airlift pumping effect and boost heat transfer coefficient exterior to condenser tube banks. It is composed of

*Corresponding author. Email: haiteng.ma@sjtu.edu.cn

two parts, as shown in Figure 1. Air cooled condenser at the bottom is responsible to produce distilled water from the steam at the tube inlet, which could alleviate the shortage of drinking water in arid countries. Air heater at the top is added to enhance thermal chimney effect, by collecting waste heat from various sources (power plant, HVAC, etc.) and ducting it through the tubes. Air heater is designed to drag more ambient air upwards at a higher speed, so that heat transfer exterior to air cooled condenser at the bottom is enhanced. As a whole, thermal chimney driven air cooled condenser could produce freshwater from steam and waste heat that are otherwise dumped. To simplify the design and analysis of thermal chimney driven air cooled condenser system, passive heat exchangers with bare tubes are considered in this paper, which can be treated as an array of circular cylinders.

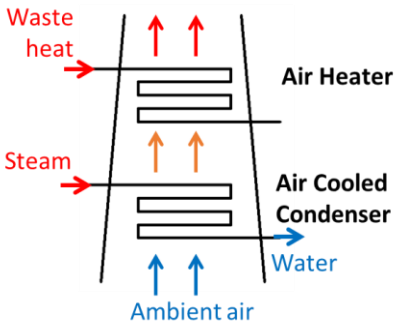

Figure 1. Schematic of the thermal chimney driven air cooled condenser system

Natural convection heat transfer on the outer surface of circular cylinders has been studied profusely for simple layouts. For a single heated horizontal cylinder, empirical correlations for Nusselt number on cylinder surface were presented in the classical work by Morgan [13] and Churchill and Chu [14] and more recent by Atayılmaz and Teke [15]. Kitamura et al. [16] investigated the influence of turbulent transition on free convection heat transfer of cylinders in water. They stated that Nusselt number is increased notably in the transitional and turbulent regions on the cylinder surface. Ma and He [17] found through high-fidelity large eddy simulations that laminar thermal plume leaving the single cylinder accelerates subject to work done by buoyancy force, becomes unstable and transits to turbulence as it develops.

For a single vertical column of heated cylinders, the effect of vertical spacing on heat transfer performance has been revealed by many researchers. For two vertically-aligned cylinders, Chae and Chung [18] reported natural convection heat transfer of the lower cylinder is unaffected by the change in vertical distance between the two cylinders, and exhibits identical behavior to that of a single cylinder. But for the upper cylinder, surface Nusselt number is enhanced as the vertical pitch increases, due to two physical mechanisms: preheating effect and velocity effect. Preheating of the upper cylinder is caused by the surrounding hot plume rising from the lower cylinder, leading to a reduced local temperature difference and thus, surface heat transfer. Meanwhile, velocity of the plume from the lower cylinder imposes certain kind of forced convection on the upper cylinder and thus, enhances heat transfer. As the vertical pitch enlarges, the preheating effect is weakened and the velocity effect is strengthened, leading to enhanced heat transfer on the upper cylinder. Such physical insight has also been presented by Sparrow and Niethammer [19], Heo et al. [20] and Stafford and Egan [21]. In addition, thermal plumes from the upper and lower cylinders may oscillate and interact to produce strong periodicity in local heat transfer rate, as measured by Persoons et al. [22].

For a single column of three or more cylinder, Corcione [23] found through laminar simulations that heat transfer rate compared to the single-cylinder case on any downstream cylinder is augmented at small tube pitch and declined at large ones. In fact, at large vertical spacing, thermal plume is more prone to transit to turbulence, which increases heat transfer on downstream cylinders, as reported by Kitamura et al. [24].

For two vertical columns of cylinders, the effect of horizontal spacing on natural convection heat transfer has also been investigated by quite a few researchers. Corcione [25] found that as the horizontal pitch decreases from very large values, thermal chimney effect arises due to interaction between the two columns and produces a peak in Nusselt number. If the cylinders are drawn closer horizontally, heat transfer reduces owing to “merging of the two boundary layers”. Similar mechanism was also discovered by Stafford and Egan [21], which stated optimal separation distance is achieved when the boundary layers from the two cylinders touch. When the horizontal spacing between the two columns is large, thermal plume from each column acts independently, but as the horizontal spacing dwindles, coupling and interaction between the plumes from the two columns become stronger, as noted by Narayan et al. [26]. These findings are also applicable to more complex configurations such as two columns of cylinders in an enclosure (Park et al. [27]) and two horizontally-aligned cylindrical tubes with plate fins (Chen et al. [28]).

However, for a complete array of horizontal cylinders, which is representative of a heat exchanger packed with a myriad of tubes forming a large array, natural convection heat transfer research is very little in open literature. In particular, for an array with three or more columns of horizontally-aligned cylinders, natural convection heat transfer and fluid flow investigation has, to the best of the authors’ knowledge, not been reported in open literature, but is relevant to the design of compact passive heat exchangers.

As such, the common practice in passive heat exchanger design is to adopt heat transfer correlations of tube banks in forced convection. For instance, the classical correlation of Briggs and Young [29] is used to calculate heat transfer coefficient on the outer surface of natural draft air cooled condenser by Zhao et al. [3] in nuclear and Zou et al. [10] in

geothermal power plants, although it is regressed from forced convection data with a Reynolds number between 1,000 to 20,000. This approach is questionable because Reynolds number in passive heat exchanger usually falls below the range of validity for the forced convection correlations, as stated by Gyles et al. [30]. More reliable method to predict natural convection heat transfer of tube banks, such as computational fluid dynamics (CFD) simulation, is required for even the simplest bare tubes.

To address these issues, this paper develops a combined steady and unsteady Reynolds-Averaged Navier-Stokes (RANS) approach to investigate natural draft and heat transfer of thermal chimney system comprised of one row or two rows of horizontal cylinders with multiple columns. The numerical method is verified for mesh and time step sensitivity, and validated against particle-image velocimetry (PIV) and heat transfer measurement data. Next, the effect of horizontal and vertical pitches on thermal chimney performance is explored by RANS simulations, due to its fast computational speed. Some interesting thermo-fluids behaviors are spotted, analyzed and further substantiated by URANS simulations. The implications for thermal chimney system design are also explained.

2. EXPERIMENTAL SETUP

Experimental thermal chimney model with a rectangular cross-section (280 mm×190 mm) was constructed by four pieces of transparent acrylic sheets (5 mm thickness) and an aluminum frame. The model is 730 mm high and lifted 200 mm above ground to allow ventilation from the bottom. Ten cylindrical cartridge heaters, whose diameter (*D*) is 16 mm and length is 190 mm, with embedded K-type thermocouples were installed at the front and back sheets, as shown in Figure 2. They are placed 200 mm (12.5*D*) above the bottom of thermal chimney model. Temperature of each embedded thermocouple probe is controlled to be constant at 373 K by an OMEGA™ PID (proportional integral derivative) controller. The cylinders are made from stainless steel, whose thermal conductivity is 16.2 W/m-K at 100 ℃. Biot number based on *D*/4 is around 0.0025, so the surface temperature of each cylinder is uniform according to lumped capacitance model. Furthermore, infrared thermography on the ten cylinder surfaces confirms that temperature on each cylinder is 373±2 K except near the front and rear endwalls, as presented in Li et al. [31]. Thus, Rayleigh number, denoted as $Ra = g\beta(T_w - T_\infty)D^3/\nu\alpha$, is 1.9×10^4. Here, T_w is the temperature at cylinder surface, T_∞ is the ambient temperature, β, ν and α are coefficient of thermal expansion, kinematic viscosity and thermal diffusivity respectively, and they are evaluated at a reference temperature of $T_{ref} = (T_w + T_\infty)/2$. The cylinder surfaces are polished to minimize the emissivity ($\varepsilon \approx 0.1$), so the radiation heat transfer from the cylinders is negligible.

PIV measurements of the thermal chimney models were conducted in an isolated test section which was placed in a stagnant wind tunnel so that the seeding particles can be safely exhausted, as shown in Figure 2. Velocity measurements were taken in the mid-span plane across the heaters. Airflow inside the chimney was illuminated by the PIV laser and a high-speed camera was used to capture the field of view. The seeding was a fine mist with a nominal particle diameter of 0.2 μm provided by a smoke generator. The PIV laser light sheet was directed from the top ceiling to cover the mid-span plane of the chimney. It is a Litron dual cavity Nd:YAG laser capable of providing 100 mJ pulses of 8 ns duration at a maximum repetition rate of 200 Hz. The time delay between image pairs was set to 2.2 ms in order to appropriately resolve the velocity of buoyant plume above the cylinder array. A 4M pixel Phantom v341 camera digital video camera was used for PIV image recording, and 600 image pairs at a rate of 200 Hz over 3 seconds were taken for each experimental configuration. The raw data were post processed in LaVision Davis 8 and MATLAB environment. Uncertainty of the measured velocity is mainly decided by the accuracy of PIV set, which is estimated to be $= \frac{0.1}{M\Delta t} = 0.008$ m/s, where M (=5.5 pixels/mm) represents the image magnification factor and Δt (=2.2 s) is the laser pulse delay.

The thermal chimney models with one row and two rows of heated cylinders were measured by PIV. For the one-row configuration, ten cylindrical heaters are evenly distributed with a fixed horizontal pitch of P_h=1.75*D*, which was determined according to preliminary CFD analyses by Ma et al. [32]. For the two-row configuration, airflow velocity of thermal chimney with three vertical pitches (P_v=2*D*, 5*D* and 8*D*) was measured, where the horizontal pitch is fixed at P_h=1.75*D*. Detailed experimental data were reported in a preceding paper by Yu et al. [33]. They are used to validate CFD method in the present study.

Heat transfer measurements were also conducted on the one-row configuration, by varying the surface temperature of circular cylinders from 313 K to 413 K with an interval of 20 K, hence Rayleigh number changes from 0.74×10^4 to 2.20×10^4. The power input and surface temperature of each cylinder was controlled and measured through individual power meter and thermocouple. Heat transfer coefficient is defined as $h = q''/(T_w - T_\infty)$, where q'' is the surface heat flux. It can be represented by the non-dimensional Nusselt number, denoted as $Nu=hD/k$, where k is thermal conductivity of fluid evaluated at a reference temperature of $T_{ref} = (T_w + T_\infty)/2$. Average heat flux on the cylinders in thermal chimney is obtained through dividing the total power input by the total surface area, so the average heat transfer coefficient (h_{avg}) and Nusselt number (Nu_{avg}) is derived subsequently. Uncertainty of the average Nusselt number comes from the readings of the power meter (0.5%), K-type thermocouple (0.5 ℃) and the gauge for cylinder diameter (0.02 mm). Applying Taylor Series Method for uncertainty propagation (Coleman and Steele [34]), the maximum uncertainty of average Nusselt number is ±4.5%.

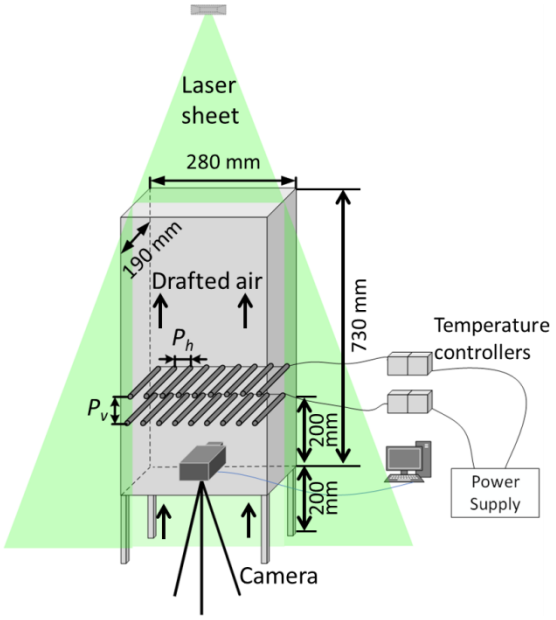

Figure 2. Setup of the thermal chimney test section and PIV measurement

3. NUMERICAL SETUP, VERIFICATION AND VALIDATION

3.1 Theoretical Formulations

Numerical simulations of natural convection heat transfer and fluid flow use Boussinesq approximation to account for buoyancy effect, which treats fluid density as invariant except in body force term of momentum equation. This assumption is regularly adopted in buoyant simulations (Webb and Mansour [35], Grafsrønningen and Jensen [36]). The governing continuity, momentum and energy equations can then be written as:

$$\frac{\partial u_i}{\partial x_i} = 0 \tag{1}$$

$$\frac{\partial u_i}{\partial t} + u_j \frac{\partial u_i}{\partial x_j} = -\frac{1}{\rho_0}\frac{\partial p}{\partial x_i} + \frac{\partial}{\partial x_j}\left(\nu \frac{\partial u_i}{\partial x_j}\right) + \beta g_i \Delta T \tag{2}$$

$$\frac{\partial T}{\partial t} + u_j \frac{\partial T}{\partial x_j} = \frac{\partial}{\partial x_j}(\alpha \frac{\partial T}{\partial x_j}) \tag{3}$$

, where temperature excess $\Delta T = T - T_\infty$ and β is thermal expansion coefficient (1/K).

Decomposing the flow variables into the mean and fluctuating component,

$$u_i = U_i + u_i' \tag{4}$$

$$T = \bar{T} + T' \tag{5}$$

, then the Reynolds-Averaged Navier-Stokes (RANS) equation gives,

$$\frac{\partial U_i}{\partial x_i} = 0 \tag{6}$$

$$\frac{\partial U_i}{\partial t} + \frac{\partial (U_i U_j)}{\partial x_j} = -\frac{1}{\rho_0}\frac{\partial P}{\partial x_i} + \frac{\partial}{\partial x_j}\left(\nu \frac{\partial U_i}{\partial x_j}\right) + \beta g_i \overline{\Delta T} - \frac{\partial (\overline{u_i' u_j'})}{\partial x_j} \tag{7}$$

According to turbulent-viscosity hypothesis (Pope [37]), the Reynolds stress is expressed as

$$\overline{u_i' u_j'} = \frac{2}{3} k \delta_{ij} - 2\nu_t S_{ij} \tag{8}$$

, where k is turbulent kinetic energy ($\frac{1}{2}\overline{u_i' u_i'}$), S_{ij} is mean strain rate tensor ($=\frac{1}{2}(\frac{\partial U_i}{\partial x_j} + \frac{\partial U_j}{\partial x_i})$), and ν_t is turbulent/eddy viscosity. As an effort to close the RANS equations, various turbulence models have been proposed over the past decades. In this paper, six RANS models are studied to assess their performance in resolving the laminar-to-turbulence transition in buoyant plumes: k-ε realizable, k-ε RNG, k-ω SST, transition SST, transition-k-kl-ω and Reynolds stress models, which will be detailed in Section 3.2. Governing equations for transition SST model, which is finally chosen in the present study according to experimental validation in Section 3.2, are briefly introduced here. In $k-\omega$ based models, the dynamic turbulent/eddy viscosity is computed as

$$\mu_t = \rho \nu_t = \rho\, k/\omega \tag{9}$$

, where k is turbulent kinetic energy and ω is specific turbulent dissipation rate. In transition SST model, k is determined by correcting the corresponding equation in $k-\omega$ SST model as

$$\frac{\partial}{\partial t}(\rho k) + \frac{\partial}{\partial x_j}(\rho k u_j) = \widetilde{P_k} - \widetilde{D_k} + \frac{\partial}{\partial x_j}[(\mu + \sigma_k \mu_t)\frac{\partial k}{\partial x_j}] \tag{10}$$

$$\widetilde{P_k} = \gamma_{eff} P_k \tag{11}$$

$$\widetilde{D_k} = \min[\max(\gamma_{eff}, 0.1), 1] \cdot D_k \tag{12}$$

, and ω is determined from the same equation in $k-\omega$ SST model as

$$\frac{\partial}{\partial t}(\rho \omega) + \frac{\partial}{\partial x_j}(\rho \omega u_j) = \alpha \frac{P_k}{\nu_t} - D_\omega + Cd_\omega + \frac{\partial}{\partial x_j}[(\mu + \sigma_k \mu_t)\frac{\partial \omega}{\partial x_j}] \tag{13}$$

, where P_k and D_ω are the production and destruction terms in the original equations of $k-\omega$ SST model, and γ_{eff} is the effective intermittency derived as

$$\gamma_{sep} = \min(s_1 \max[(\frac{Re_v}{2.193 Re_{\theta c}}) - 1, 0] F_{reattach}, 5) \cdot F_{\theta t} \tag{14}$$

$$F_{reattach} = \exp[-(R_T/15)^4] \tag{15}$$

$$\gamma_{eff} = \max(\gamma, \gamma_{sep}) \tag{16}$$

Transition SST model adds two governing equations to $k-\omega$ SST model for closure. The first additional governing equation is the transport equation for intermittency (γ),

$$\frac{\partial}{\partial t}(\rho \gamma) + \frac{\partial}{\partial x_j}(\rho \gamma U_j) = P_{\gamma 1} - E_{\gamma 1} + P_{\gamma 2} - E_{\gamma 2} + \frac{\partial}{\partial x_j}[(\mu + \frac{\mu_t}{\sigma_f})\frac{\partial \gamma}{\partial x_j}] \tag{17}$$

The second is the transport equation for momentum thickness Reynolds number ($Re_{\theta t}$)

$$\frac{\partial}{\partial t}(\rho\widetilde{Re}_{\theta t}) + \frac{\partial}{\partial x_j}(\rho\widetilde{Re}_{\theta t}U_j) = P_{\theta t} + \frac{\partial}{\partial x_j}[\sigma_\theta(\mu + \mu_t)\frac{\partial \widetilde{Re}_{\theta t}}{\partial x_j}] \quad (18)$$

Detailed explanation of the above equations and the meaning/determination of each term is presented by Menter et al. [38], where transition SST model is originally proposed.

Averaging of the energy equation (3) gives

$$\frac{\partial \bar{T}}{\partial t} + \frac{\partial(\bar{T}U_j)}{\partial x_j} = \frac{\partial}{\partial x_j}(\alpha\frac{\partial \bar{T}}{\partial x_j}) - \frac{\partial(\overline{T'u_j'})}{\partial x_j} \quad (19)$$

$$\overline{T'u_j'} = -\alpha_t\frac{\partial \bar{T}}{\partial x_j} \quad (20)$$

, where α_t is turbulent thermal diffusivity and can be determined from turbulent Prandtl number.

For the natural convection problem in this paper, boundary condition on the cylinder surface is: $u_i = 0$, T=T_w for thermal chimney cases and $q'' = -k\frac{\partial T}{\partial n} = 0$ for the single cylinder case. On the bottom boundary of computational domain, P_t=1 atm, T_t=293 K; while on the top boundary, P_s=1 atm.

3.2 Natural Convection around a Single Horizontal Cylinder

Numerical simulations are first carried out for the simplest case of natural convection around a single horizontal cylinder to calibrate the performance of six different RANS models in predicting the transitional behavior of buoyant plume, based on the measurement data of Grafsrønningen et al. [39]. The numerical domain, mesh, boundary condition, solver setting and experimental validation have been elaborated in the previous work by Ma and He [17], and will be restated briefly in this section.

Numerical settings are chosen to represent the experiment of Grafsrønningen et al. [39] wherever possible. The cylinder surface is a non-slip wall whose heat flux is kept constant (11.1 kW/m^2). Pressure inlet with a total pressure of 1 atm and total temperature of 293 K is imposed on the bottom boundary, while pressure outlet with a static pressure of 1 atm is imposed on the top and lateral boundaries. The cylinder is immersed in water with constant properties assessed at 293 K. Rayleigh number in this case is 8×10^7, so thermal plume is believed to undergo transition to turbulence at certain distance above the heated cylinder, according to Grafsrønningen et al. [39].

Computations are implemented by the pressure based solver in ANSYS Fluent 2020R1, whose pressure-velocity coupling is achieved by SIMPLEC algorithm. Gravity is included by imposing a downward acceleration of 9.8 m^2/s^2 in vertical axis. Pressure, gradient, momentum and energy equations are discretized by body force weighted, least squares cell based, bounded central differencing and second order upwind schemes, respectively.

3.2.1 Mesh Independence

Parameters of mesh dependency study for the single cylinder case are listed in Table 1. Average y_+ on cylinder is far below 1 so the wall boundary layer is properly resolved. Average heat transfer coefficient converges as mesh resolution increases. Figure 3 contours difference in velocity magnitude between different grid sizes. Variance between the 125,000 and 154,000 grid sizes is lower than that between the 93,000 and 125,000 grid sizes. Thus, a mesh resolution of 125,000 is adequate for the two-dimensional RANS computation of the single cylinder.

Table 1. Parameters of mesh independence study (one single cylinder)

Grid size	Nodes on cylinder	y_{min} on cylinder [mm]	$y_{+,avg}$ on cylinder	h_{avg} [W/m^2-K]
93,000	160	0.02	0.042	482.893
125,000	176	0.01	0.021	483.010
154,000	216	0.007	0.015	483.084

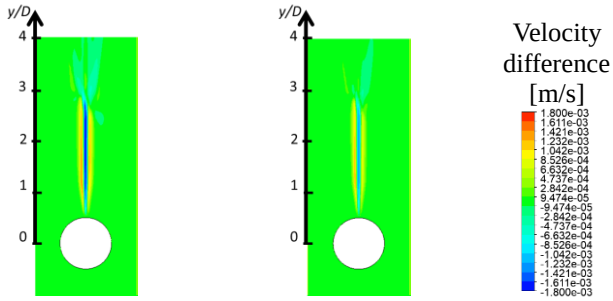

(a) (93,000-125,000) (b) (125,000-154,000)

Figure 3. Difference of velocity magnitude between different mesh sizes for a single cylinder

3.2.2 Validation Against Experimental Data

Figure 4 shows the Nusselt number distribution along the circumference of a single cylinder. Surface heat transfer results from six RANS models are almost the same. This is because the flow stays laminar around the cylinder, as indicated by the steady decrease of Nusselt number from the lowest point to the top of the cylinder. CFD results agree with experimental data (Grafsrønningen et al. [39]) by a margin of 5% in large portion of the cylinder, which is within measurement uncertainty. Near the cylinder top (θ=[160 °, 180 °]), difference between CFD and experiment is relatively large due to separation of thermal boundary layer when forming the buoyant plume (Kuehner et al. [40]). Such discrepancy has also been reported by Pelletier et al. [41].

Figure 5 plots mean velocity magnitude of buoyant plume along horizontal x-axis at 3.52D downstream cylinder center, where thermal plume has undergone transition to turbulence. Compared to PIV measurement data by Grafsrønningen et al. [39], transition SST model shows the closest agreement among six RANS models. Maximum discrepancy in velocity magnitude is 25% and occurs at the centerline (x=0). Plume width is also predicted satisfactorily. As a contrast, k-ω SST

and transition-*k*-*kl*-ω models overpredict centerline velocity by above 60% and underpredict plume width conspicuously. *k*-ε realizable, *k*-ε RNG and Reynolds stress models fail to capture plume width. Although previous studies suggest *k*-ε RNG (Chen et al. [42]), zero-equation model (Chen et al. [28]) or laminar model (Stafford and Egan [21], Park et al. [27]) performs well in simulating natural convection heat transfer around horizontal tubes, the selection of proper flow model does depend on the geometry and physics of interest. When considering the fluid flow field, particularly the laminar-to-turbulent transition associated with buoyant plume, Figure 5 demonstrates that transition SST is the most suitable RANS model and thus, will be employed in the following simulations.

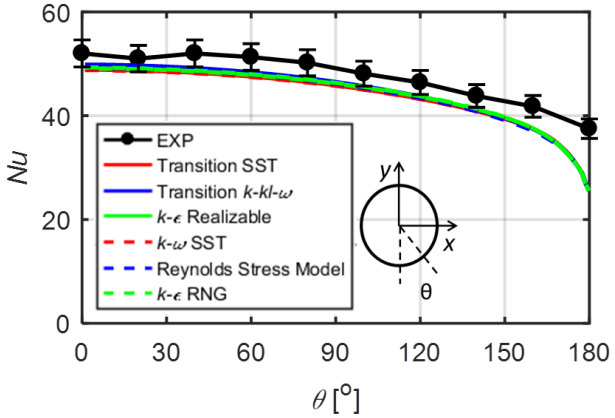

Figure 4. Nusselt number on circumference of a single cylinder at a Rayleigh number of 8×10^7 from experiment (Grafsrønningen et al. [39]) and 6 RANS models in the present CFD

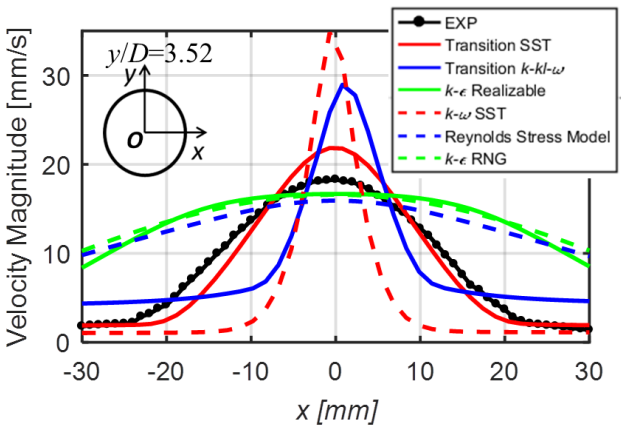

Figure 5. Mean velocity magnitude along the horizontal *x*-axis at *y*/*D*=3.52 from experiment (Grafsrønningen et al. [39]) and 6 RANS models in the present CFD for a single horizontal cylinder

3.3 Thermal Chimney of Multiple Cylinder Columns in One Row

Built upon the simplest case with a single heated cylinder, numerical simulations are then carried out for thermal chimney layouts that are measured experimentally, as described in Section 2. Computational domain, mesh and boundary condition for the thermal chimney system simulation are illustrated in Figure 6. According to the previous three-dimensional numerical study of the present test rig, flow velocity and cylinder temperature are basically invariant along the direction of cylinder axis except in limited regions near the front and back chimney walls (Li et al. [31]). In another word, influence of boundary layer on the front and back endwalls is negligible near the mid-span of chimney tubes. Therefore, a two-dimensional computational domain is adopted, with the top and bottom boundary located at 32.5*D* and 12.5*D* downstream and upstream of cylinder center respectively, which is the same as the experimental thermal chimney model.

Structured mesh with a grid size of 216,000 is employed, according to mesh dependence study in Section 3.3.1. Boundary condition on the bottom of the domain is specified as pressure inlet with a total pressure of 1 atm at room temperature (293 K). On the top boundary, pressure outlet with a static pressure of 1 atm is imposed. Such boundary condition setup has been employed and validated by Ma and He [17], Heo et al. [20] and Sebastian and Shine [43]. On the cylinder surface, non-slip wall with isothermal boundary condition (T_w=373 K) is specified.

As shown in Figure 6, the two-dimensional computational domain is extracted for the central six cylinders with periodic lateral boundary conditions, so as to avoid the influence of boundary layers on the left and right endwalls. Justification for this modelling approach will be demonstrated in Section 3.4. In fact, this computational model is representative of real thermal chimney products such as natural draft air cooled condensers, whose tubes form a large array of horizontal cylinders and hence, the effect of chimney wall boundary layer on the main flow field is negligible.

The thermal chimney model is placed in air at room temperature (293 K). The fluid is modelled as air with constant physical properties (viscosity, thermal conductivity and specific heat), similar to the approach employed by Corcione [23, 25], Park et al. [27], Chen et al. [28]. Transition SST model is used to account for laminar-to-turbulent flow transitioning, according to the validation study in Section 3.2. Solver settings are kept the same as Section 3.2 unless otherwise stated. Due to the unsteadiness of interaction between buoyant plume from each cylinder, oscillations in monitored flow quantities may be observed during the solution process. Thus, RANS results are averaged over 1000 iterations after the solution residual cannot decrease any more, and the residual for continuity, momentum and energy equation is on the level of 10^{-2}, 10^{-3}, 10^{-6}, respectively. The net imbalance of overall mass and heat transfer through the domain boundaries is within 0.5%.

Complementary URANS calculations are then performed to reaffirm major findings made by RANS, as discussed later in this section. The residual for continuity, momentum and energy equation at each time step in URANS is reduced to the level of 10^{-3}, 10^{-5}, 10^{-7}, respectively.

Both low and high Rayleigh numbers are tested in the following simulations. The low Rayleigh number cases (Ra=1.9×10^4) are used to validate the CFD method against experimental measurement depicted in Section 2, so cylinder diameter and temperature are the same as experimental setup. Characteristic velocity ($V_0 = \sqrt{g\beta D(T_w - T_\infty)}$) is 0.21 m/s. For the high Rayleigh number cases (Ra=3.3×10^5), cylinders have a diameter of 40 mm and constant temperature of 393 K, so the characteristic velocity is 0.37 m/s.

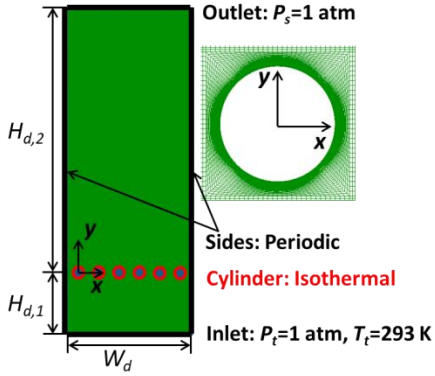

Figure 6. Computational domain, mesh and boundary condition for the thermal chimney system

3.3.1 Mesh Independence

Parameters for mesh independence study are listed in Table 2. Average y_+ on cylinder is well below 1 so the wall boundary layer is properly resolved. Average heat transfer coefficient converges as mesh resolution increases. Grid convergence index between the coarsest and the medium meshes is 1.9%, while it is 1.3% between the finest and the medium meshes, computed through Richardson extrapolation. So the solutions are in the asymptotic range of convergence. Figure 7 illustrates difference in velocity magnitude among the three grid sizes. Discrepancy between the finest and the medium grids is smaller than that between the coarsest and the medium grids. Therefore, the grid size of 216,000 is adequate for the two-dimensional RANS simulations in this study.

Table 2. Parameters for mesh independence study (one-row of cylinders)

Grid size	Nodes on cylinder	y_{min} on cylinder [mm]	$y_{+,avg}$ on cylinder	h_{avg} [W/m^2-K]
146,000	100	0.005	0.01383	19.28
216,000	120	0.0025	0.00693	19.16
322,000	160	0.001	0.00275	19.06

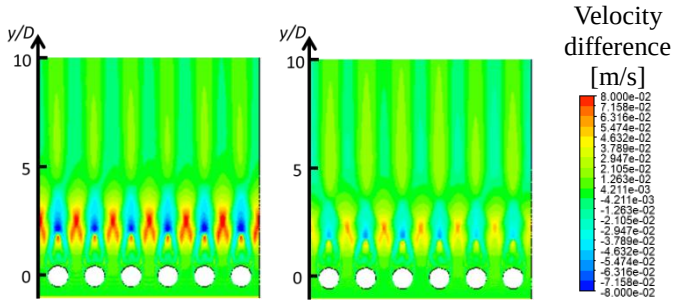

(c) (146,000-216,000) (d) (216,000-322,000)

Figure 7. Difference of velocity magnitude between different mesh sizes for the one-row thermal chimney system

3.3.2 Time Step Independence

To cross-validate key findings of RANS computations, URANS simulations are also implemented. Results from steady solver are used for the initialization of unsteady solver. Transient formulation is based on first order implicit scheme. URANS results are averaged over a physical time of 50 s, corresponding to roughly 15 flow-through times in the whole thermal chimney system, which is statistically sufficient for time-averaging. Three time step sizes (Δt=0.005 s, 0.01 s, 0.02 s) are compared and their differences in mean velocity magnitude are shown in Figure 8. Discrepancy between the smallest and the medium time step sizes is smaller than that between the largest and the medium time step sizes. Hence, time step size is chosen to be 0.01 s for URANS computations.

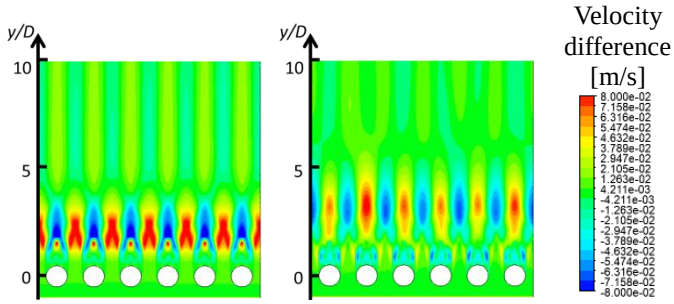

(a) (Δt=0.02-0.01 s) (b) (Δt=0.01-0.005 s)

Figure 8. Difference of mean velocity magnitude between cases with various time step sizes in URANS (results averaged over 50 s)

3.3.3 Validation Against Experimental Data

Based on PIV measurements depicted in Section 2, numerical simulations are validated in terms of horizontally-averaged velocity magnitude at four vertical locations, as listed in Table 3. RANS results (averaged over 1000 iterations) deviate from experimental data with a maximum of 19%. In contrast, URANS results (averaged over 50 s physical time) differ from experimental measurement by a maximum of 25%. Although the geometry of the computational domain seems simple, the flow physics of buoyant plume is quite complicated. Thermal plume is inherently weak and prone to instability, which will trigger transition to turbulence as it develops (Ma and He [17], Kitamura et al. [24]). Moreover, plume from

adjacent cylinders interacts strongly with each other and might affect the flow instability. Even for the simplest case of natural convection around a single heated horizontal cylinder, a numerical error of 52% to 143% in terms of velocity magnitude at the plume centerline is reported by Grafsrønningen and Jensen [36] in their large eddy simulations. This error was reduced to 15%-48% through tuning the domain boundary conditions in the large eddy simulations presented by Ma and He [17]. Under these contexts, CFD errors in the present RANS and URANS computations are both acceptable.

Given that steady solver reduces computational cost by at least 30 times compared to the unsteady counterpart, RANS simulations with results averaging over iterations to account for unsteady oscillations is a fast and efficient tool for the parametric study in this paper. Plausibility of key findings is guaranteed through targeted URANS simulations.

Figure 9 plots the average Nusselt number in the one-row layout with error bars, obtained from heat transfer measurements in Section 2, as well as RANS results averaged over 1,000 iterations. CFD results show the same qualitative trend with experimental data, i.e. Nusselt number increases with higher Rayleigh number. Quantitatively speaking, RANS results are lower than experimental measurements by a maximum of 10%. Given that experimental uncertainty is ±4.5%, this prediction error is acceptable.

Table 3. Horizontally-averaged velocity magnitude (m/s) at four vertical locations for thermal chimney in one row with a horizontal pitch (P_h) of 1.75D

y/D	EXP	CFD (RANS)	Relative error	CFD (URANS)	Relative error
5	0.237	0.274	16%	0.285	21%
10	0.230	0.274	19%	0.287	25%
15	0.243	0.274	13%	0.287	18%
20	0.255	0.273	7%	0.287	12%

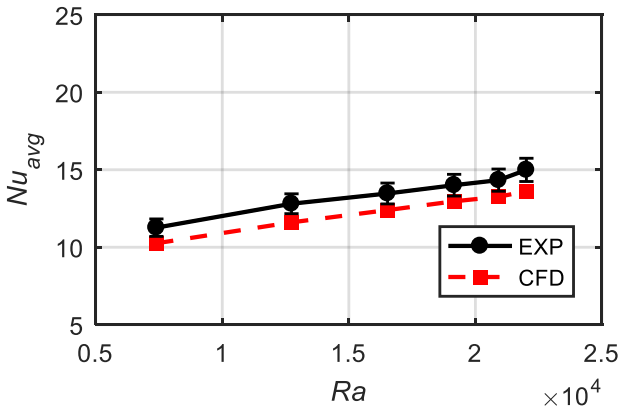

Figure 9. Average Nusselt number in the one-row configuration (horizontal pitch P_h=1.75D) at varying Rayleigh numbers

3.4 Thermal Chimney With Multiple Cylinder Columns in Two Rows

Numerical simulations are also conducted for thermal chimney with two rows of cylinders, and validated by PIV measurements introduced in Section 2. Figure 10 contours velocity magnitude (V) for the two-row thermal chimney layout with a vertical pitch of P_v=5D and a horizontal pitch of P_h=1.75D, obtained from PIV measurement on the mid-span of chimney tubes and RANS computation (results averaged over 1000 iterations). Here, a two-dimensional numerical simulation of the whole test rig was conducted, with the lateral endwalls treated as adiabatic. It is worth mentioning that PIV measurement data exhibit relatively poor quality at the throat between adjacent cylinders and at the throat between the side cylinder and endwall. In these regions, the high-velocity jet is not properly resolved by PIV image pairs, because the laser pulse delay in PIV measurements, which is set to fit the low-velocity plume above the cylinder array, is too large to deal with the high-velocity jet at the throats. Nevertheless, in other regions of the measurement plane, the PIV data are well-processed and show several qualitative trends that are consistent with the CFD results. A strip of low velocity region exists downstream of each cylinder in the lower and upper row, corresponding to the wake past the cylinder. Between each wake, relatively high velocity area is observed. Moreover, boundary layer on the two lateral walls only influences plume development of the leftmost and the rightmost cylinders. Flow field around the middle cylinders is basically periodic and unaffected by the endwall boundary layers. Therefore, the domain modelling approach in the present study, i.e. selecting six cylinders in the middle and imposing periodic condition on lateral boundaries (shown as the dashed box in Figure 10), is justifiable.

Table 4 lists horizontally-averaged velocity magnitude at four vertical locations in the two-row thermal chimney model with a fixed horizontal pitch (P_h) of 1.75D and different vertical pitches (P_v=2D, 5D, 8D). Origin in vertical coordinate coincides with the center of lower cylinders. The four locations are situated above/downstream the upper cylinders by a distance of 5D, 10D, 15D and 20D respectively. It is seen that the discrepancy between experimental data and RANS results (averaged over 1000 iterations) is within 16% for all cases. For the case where the two rows are vertically separated by a distance of 2D, relative errors in RANS simulation are all within 5%. Therefore, the present numerical approach can be trusted to reproduce airflow field in thermal chimney.

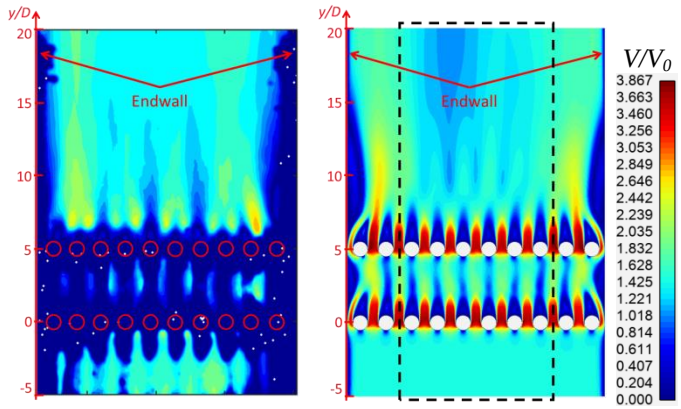

(a) PIV measurement (b) CFD

Figure 10. Velocity magnitude for the two-row layout with a vertical pitch (P_v) of 5D and a horizontal pitch (P_h) of 1.75D from (a) PIV measurement on the mid-span of chimney tubes and (b) CFD (RANS averaged over 1,000 iterations)

Table 4. Horizontally-averaged velocity magnitude (m/s) at four vertical locations for thermal chimney in two rows with a horizontal pitch (P_h) of 1.75D

y		P_v+5D	P_v+10D	P_v+15D	P_v+20D
P_v =2D	EXP	0.331	0.344	0.346	0.354
	CFD (RANS)	0.339	0.334	0.334	0.334
	Error	2%	-3%	-3%	-5%
P_v =5D	EXP	0.322	0.318	0.335	0.358
	CFD (RANS)	0.301	0.300	0.300	0.300
	Error	-7%	-6%	-11%	-16%
P_v =8D	EXP	0.331	0.342	0.354	N/A
	CFD (RANS)	0.316	0.306	0.306	0.305
	Error	-5%	-11%	-14%	N/A

4. NUMERICAL RESULTS AND ANALYSES

Up to this point, the numerical method to model thermal chimney with multiple cylinder columns in one row and two rows has been established and validated based on PIV and heat transfer measurements. Now it will be utilized in the following parametric study, focusing on the effects of horizontal and vertical pitches on the natural draft and heat transfer of thermal chimney system.

4.1 Effect of Horizontal Pitch

Effect of horizontal pitch is investigated on the one-row thermal chimney model. Upward velocity is induced by natural draft from the array of heated cylinders throughout the thermal chimney model. At the bottom boundary of the computational domain, the local flow velocity is characterized by Reynolds number, $Re_b = V_{y,b}D/\nu$, where $V_{y,b}$ is the mass-averaged upward velocity at the bottom boundary and ν is the kinematic viscosity. Re_b is in fact an indicator of the strength of natural draft which pumps the air upward. Its variation with respect to the dimensionless horizontal pitch (P_h/D) is graphed in Figure 11. An optimal horizontal spacing exists for the natural draft strength at both the low and high Rayleigh numbers, due to the balance between two counteracting mechanisms: chimney effect and blockage effect. As the horizontal pitch reduces, chimney effect is augmented due to stronger interaction between adjacent cylinders, which acts to enhance the natural draft strength. Meanwhile, blockage effect is also promoted due to the merging of boundary layers on adjacent cylinders (Corcione [25]), which serves to undermine the natural draft strength.

At the low Rayleigh number (Ra=1.9×10^4), natural draft strength increases as P_h/D reduces from 6 to 2.5, because chimney effect prevails over blockage effect. But as P_h/D reduces further, natural draft strength decreases notably due to the predominance of blockage effect. Hence the optimal spacing for the strongest natural draft is P_h/D=2.5. At the high Rayleigh number (Ra=3.3 × 10^5), similarly, natural draft strength, as indicated by Re_b, first rises and then reduces with closer horizontal pitch. But the optimal spacing changes to P_h/D=1.75.

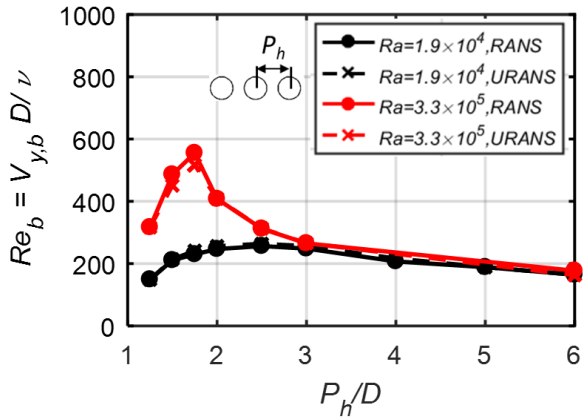

Figure 11. Reynolds number based on mass-averaged upward velocity at the bottom boundary (Re_b), versus horizontal pitch (P_h) for cylinders in one row, from RANS (averaged over 1,000 iterations) and URANS (averaged over 50 s) results

To illustrate the flow field produced by natural draft of the array of heated cylinders, Figure 12 contours the upward velocity at two selected horizontal pitches for the low Rayleigh number case (Ra=1.9×10^4), obtained from URANS results averaged over 50 s. The flow pattern changes qualitatively at these two spacings. When cylinders are placed far away from each other horizontally (P_h/D=4), flow field is dominated by thermal plume that is clearly identifiable downstream of each cylinder, with an upward velocity that is larger than or comparable to that at the throat between cylinders. It is expected that at very large horizontal pitch, each cylinder acts independently and induces a buoyant plume downstream separately, whose pattern resembles that in a single horizontal

cylinder presented by Kitamura et al. [24] and Ma and He [17]. When cylinders are drawn closer to each other, i.e. at P_h/D=2.5, flow field is dominated by thermal chimney effect caused by enhanced interaction between cylinders. As a result, the high velocity region manifests at the throat between cylinders, and the striped thermal plume is no longer observable. Flow mechanism regarding the effect of horizontal pitch in multiple columns of cylinders is similar to that in two columns, which was reported by Stafford and Egan [21], Park et al. [27], Chen et al. [28] and Narayan et al. [26]. One slight difference with the two-column scenario is, the buoyant plumes are not tilted inward in the vertical direction, due to the interaction among multiple columns.

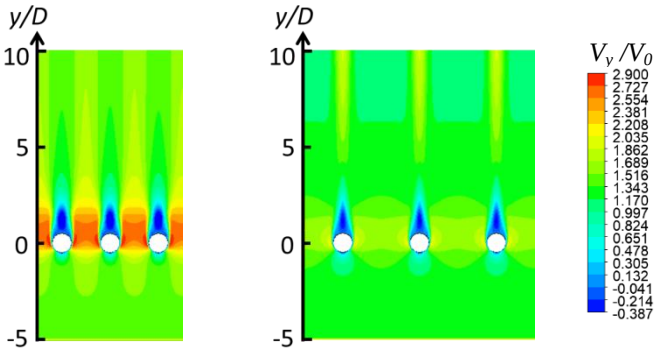

(a) P_h/D=2.5 (b) P_h/D=4

Figure 12. Upward velocity (V_y) for cylinders in one row at Ra=1.9×10^4 (URANS results averaged over 50 s)

For the case with high Rayleigh number (Ra=3.3×10^5), upward velocity contours at two horizontal pitches are shown in Figure 13, whose results are obtained by URANS averaged over 50 s. At small horizontal pitch (P_h/D=1.75), dominant mode of flow field is chimney formed by interaction between adjacent cylinders, while at large horizontal pitch (P_h/D=2.5), airflow is dominated by thermal plume above each discrete cylinder. Qualitative patterns of these two modes are similar to that at low Rayleigh number (Figure 12).

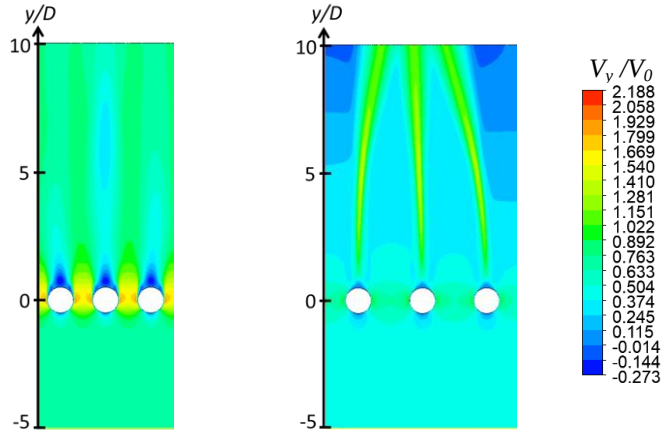

(a) P_h/D=1.75 (b) P_h/D=2.5

Figure 13. Upward velocity (V_y) for cylinders in one row at Ra=3.3×10^5 (URANS averaged over 50 s)

Having established the alteration of flow dominant mode with respect to horizontal spacing, now let us return to Figure 11 for more detailed analyses. It is seen that at the high Rayleigh number (Ra=3.3×10^5), Re_b is 7%-20% bigger than that at the low Rayleigh number (Ra=1.9 × 10^4) when the horizontal pitch is large ($P_h/D \geqslant 2.5$). At these horizontal pitches, the flow field for the high Rayleigh number case is dominated by discrete plume from each cylinder (shown in Figure 13b), which tends to develop independently from each other. When the horizontal pitch is small ($P_h/D \leqslant 2$), Re_b at the high Rayleigh number is 65%-140% bigger than that at the low Rayleigh number, indicating the natural draft or airlift pumping is much stronger. This is because the chimney effect initiates and grows gradually for the high Rayleigh number case (shown in Figure 13a), as the interaction between adjacent cylinders is enhanced at shorter horizontal distances. Another notable observation from Figure 11 is the optimum pitch for the strongest natural draft is smaller at the high Rayleigh number. This is because chimney effect manifests at shorter horizontal distance for the high Rayleigh number case. Transition of the flow pattern from plume-dominant mode to chimney-dominant mode occurs at P_h/D=[1.75, 2.5] for the high Rayleigh number case (as shown in Figure 13), whereas it takes place at P_h/D=[2.5, 4] for the low Rayleigh number case (as shown in Figure 12). It is conjectured that at higher Rayleigh number, the striped plume above each cylinder is stronger and more resistant to interaction between adjacent cylinders, which requires closer horizontal distance to disrupt the discrete plume and elicit chimney effect.

To study heat transfer characteristics of the tube bank, Figure 14 plots the area-averaged Nusselt number (Nu_{avg}) on cylinder surfaces with respect to the dimensionless horizontal pitch (P_h/D). The area-averaged Nusselt number in the high Rayleigh number case is 40% to 50% larger than that in the low Rayleigh number case. For both the high and low Rayleigh number cases, the area-averaged Nusselt number keeps increasing as the cylinders get closer to each other, because the local flow velocity around each cylinder rises as a result of the shrinking throat area, as observed in Figure 12 and Figure 13.

As shown consistently in Figure 11 and Figure 14, results between iteration-averaged RANS and time-averaged URANS are almost the same. Again, this justifies using iteration-averaged RANS for the sensitivity and optimization study of thermal chimney external natural convection, at a much faster speed than URANS. In the next section, RANS will be used as an agile tool to investigate the effect of eight vertical pitches at five different horizontal pitches for the two-row thermal chimney system, at the high Rayleigh number of 3.3×10^5. Key findings from these 40 RANS computations are then bolstered by several representative URANS simulations.

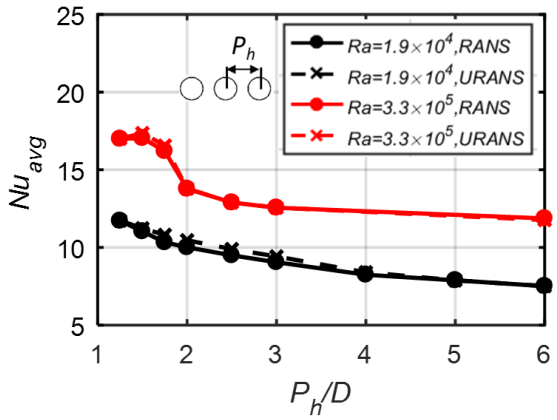

Figure 14. Average Nusselt number (Nu_{avg}) on the cylinder surfaces of the one-row thermal chimney model, versus horizontal pitch (P_h), from RANS (averaged over 1,000 iterations) and URANS (averaged over 50 s) results

4.2 Effect of Vertical Pitch

Thermal plume is more prone to instability and transition to turbulence at higher Rayleigh number, which further complicates thermo-fluids behavior of thermal chimney system. Besides, Rayleigh number in the order of 10^5 or above is frequently encountered in passive heat exchanger design. Therefore, in the rest of this paper, we will investigate fluid flow and heat transfer of thermal chimney at a Rayleigh number of 3.3×10^5.

Figure 15 plots Reynolds number based on mass-averaged upward velocity at bottom boundary of the computational domain (Re_b) versus varying vertical pitch at five different horizontal pitches. For each fixed horizontal pitch, the natural draft strength is boosted by enlarging the vertical pitch. In particular, Re_b is augmented by 80% (upward velocity at bottom boundary rises from 0.2 m/s to 0.36 m/s) when the vertical pitch increases from P_v/D=4.5 to 6 at a horizontal pitch of P_h/D=2.5, and when the vertical pitch increases from P_v/D=6 to 10 with a horizontal pitch of P_h/D=3. Physical mechanism behind this remarkable enhancement of natural draft strength will be elucidated in the last part of this section.

Figure 15 also indicates the strongest natural draft strength is achieved at P_h/D=2 when P_v/D=[0, 10] and at P_h/D=2.5 when P_v/D=[15, 20], with Re_b in the range of [680, 980], or an upward velocity of 0.35 m/s to 0.5 m/s. This draft velocity is comparable to other lab-scale natural draft studies in literature (Lu et al. [7], Tanimizu and Hooman [9]). It can be further boosted by additional measures, such as adding more cylinder rows, using tubes with larger diameter and raising the temperature of cylinders, which are beyond the scope of this paper.

On the heat transfer side, Figure 16 plots the average Nusselt number on the surfaces of the lower and upper row with varying vertical pitch at five different horizontal pitches. The average Nusselt number ge1nerally increases with larger vertical distance at a fixed horizontal pitch, due to the augmentation of natural draft velocity, as shown in Figure 15. This is different from the observation of cylinders in a single column, where the vertical pitch has no influence on the lower cylinder and the natural draft velocity from the bottom is very small, as reported by Chae and Chung [18] and Stafford and Egan [21]. In particular, for the lower row, the average Nusselt number is raised by about 20% (from 15.5 to 18) when vertical pitch increases from P_v/D=4.5 to 6 at a horizontal pitch of P_h/D=2.5, and when the vertical pitch increases from P_v/D=6 to 10 at a horizontal pitch of P_h/D=3. This is attributed to the sudden rise of natural draft strength, as noted in Figure 15, whose physical mechanism will be elaborated in the last part of this section.

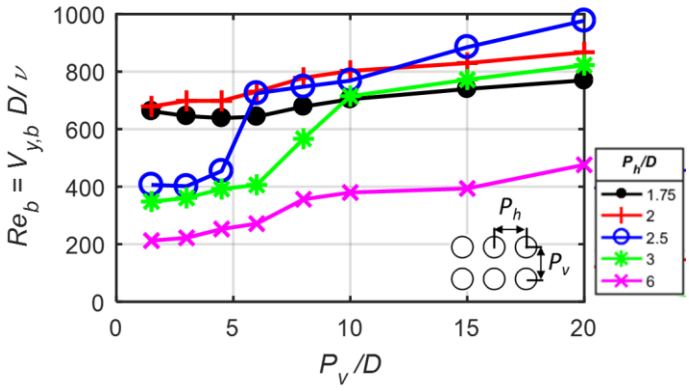

Figure 15. Reynolds number based on mass-averaged upward velocity at the bottom boundary (Re_b) versus vertical pitch (P_v) at different horizontal pitches (P_h) for cylinders in two rows with $Ra=3.3\times10^5$ (RANS averaged over 1000 iterations)

For the upper row in thermal chimney, Figure 16 shows that average Nusselt number increases with further vertical distances by a reducing slope. This is attributed to two physical mechanisms: preheating effect caused by the immersion in the hot plume from the lower cylinder, and velocity effect caused by natural draft flow field, which are essentially the same mechanisms as those of cylinders in a single column (Chae and Chung [18] and Heo et al. [20]). When the two rows are placed close to each other, preheating effect dominates so the average surface Nusselt number is quite small. As the vertical pitch rises, the preheating effect is weakened and the natural draft velocity increases, according to Figure 15. Therefore, heat transfer on the upper cylinders is enhanced. Another point worth noting is the average Nusselt number in the upper row is more sensitive to vertical pitch than the lower row, especially when the two rows are close to each other. Last but not least, qualitative trend about the variation of average Nusselt number with respect to the vertical pitch at different horizontal pitches should remain the same for other Rayleigh numbers, because the physics governing this problem are preheating and velocity effects in general.

Having established the overall trend of average upward velocity and Nusselt number in thermal chimney with varying vertical pitch, next we will investigate the underlying flow physics. Figure 17 contours upward velocity in the two-row

thermal chimney with a small horizontal pitch (P_h/D=2). At the small and large vertical pitch (P_v/D=3 and 10), flow pattern stays qualitatively the same. Natural draft field is dominated by a chimney jet at the throat between adjacent cylinders, where maximum velocity is resided. The chimney jet is caused by interaction between adjacent cylinder columns. As vertical pitch enlarges, velocity of the chimney jet increases, so does the draft velocity at the bottom boundary, as shown in Figure 15.

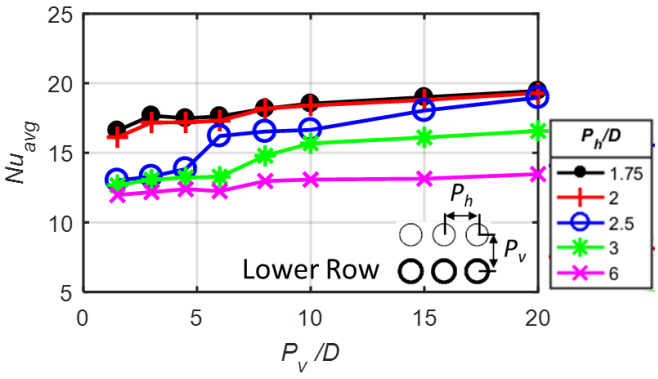

(a)

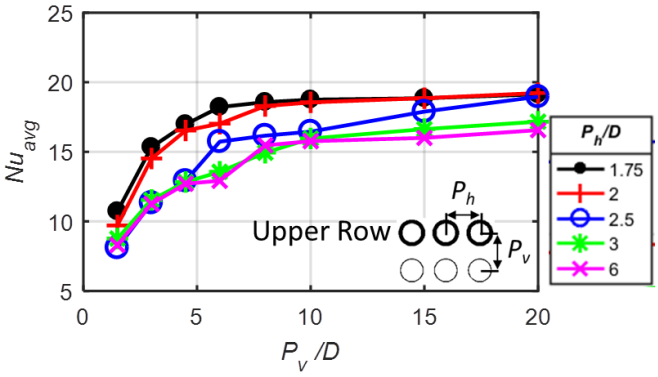

(b)

Figure 16. Average Nusselt number on the surfaces of (a) bottom row and (b) top row, with varying vertical pitch (P_v) at different horizontal pitches (P_h) for cylinder in two rows at Ra=3.3×10^5 (RANS averaged over 1000 iterations)

At a large horizontal pitch (P_h/D=6), upward velocity contours in Figure 18 shows that flow pattern is also invariant with respect to different vertical pitches. But now the natural draft is dominated by a striped buoyant plume downstream of each cylinder column, because each cylinder tends to act more independently. As vertical pitch increases, velocity in the whole flow field is raised evidently, echoing the observation in Figure 15.

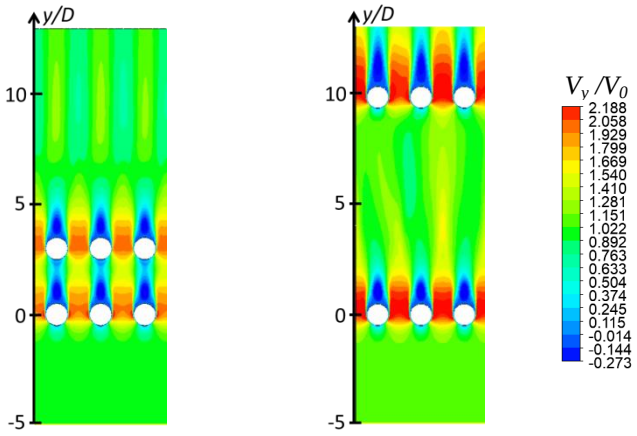

(a) P_v/D=3 (b) P_v/D=10

Figure 17. Upward velocity (V_y) for cylinders in two rows with a horizontal pitch (P_h) of 2D at Ra=3.3×10^5 (RANS averaged over 1000 iterations)

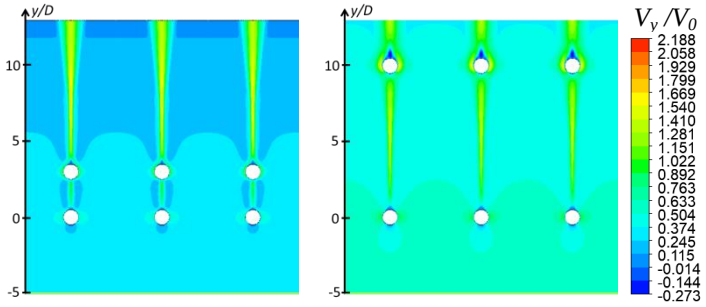

(a) P_v/D=3 (b) P_v/D=10

Figure 18. Upward velocity (V_y) for cylinders in two rows with a horizontal pitch (P_h) of 6D at Ra=3.3×10^5 (RANS averaged over 1000 iterations)

At an intermediate horizontal pitch (P_h/D=2.5), however, the dominant mode of thermal chimney could change qualitatively with vertical pitch, as shown in Figure 19. As the vertical pitch increases from P_v/D=4.5 to 6, the flow field changes from plume-dominant to chimney dominant. The buoyant plume downstream each cylinder column is weaker, while chimney jet at the throat between adjacent cylinder columns becomes stronger. The maximum upward velocity now occurs at the throat between adjacent cylinder columns, rather than at the striped plume downstream each cylinder column. For the whole flow field, the upward velocity has been boosted remarkably, leading to an abrupt increase of draft strength in Figure 15 and the heat transfer enhancement of bottom cylinders in Figure 16.

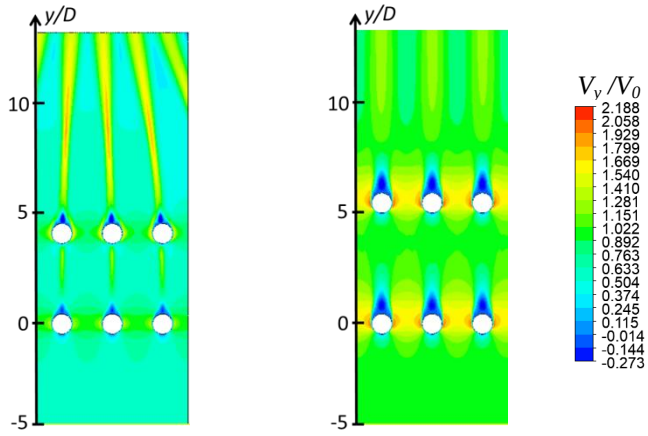

(a) P_v/D=4.5 (b) P_v/D=6

Figure 19. Upward velocity (V_y) for cylinders in two rows with a horizontal pitch (P_h) of 2.5D at Ra=3.3×10^5 (RANS averaged over 1000 iterations)

Flow pattern alteration with respect to vertical pitch at intermediate horizontal pitch is reaffirmed in the time-averaged URANS results, as shown in Figure 20. Again, the airflow field is dominated by discrete thermal plume downstream each cylinder column at small vertical pitch (P_v/D=4.5), while it is dominated by the chimney jet at the throat between adjacent cylinder columns at large vertical pitch (P_v/D=6). The upward velocity in the whole flow field is augmented conspicuously as the vertical pitch becomes bigger. In the remaining part of this paper, physical mechanism behind this distinct flow behavior will be investigated thoroughly.

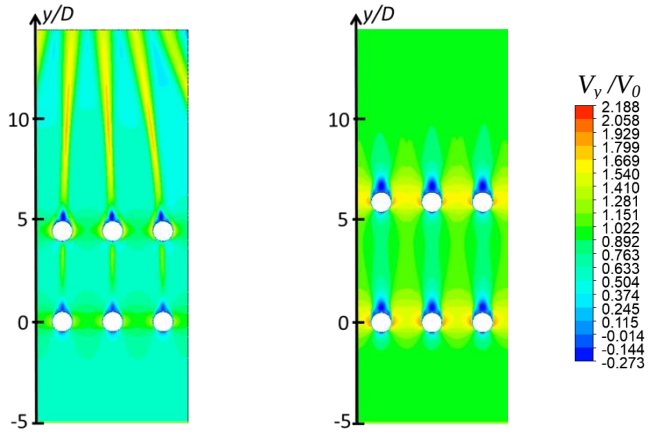

(a) P_v/D=4.5 (b) P_v/D=6

Figure 20. Upward velocity (V_y) for cylinders in two rows with a horizontal pitch (P_h) of 2.5D at Ra=3.3 × 10^5 (URANS averaged over 50 s)

Change of flow pattern with respect to the vertical pitch is also reflected in the turbulent characteristics in thermal chimney, as shown in Figure 21. At a small vertical pitch (P_v/D=4.5), turbulence onsets at a certain distance downstream of the top cylinder in each column, i.e. at a vertical coordinate of y/D=8. It is triggered by instability as thermal plume accelerates subject to work done by buoyancy force, similar to the transition mechanism of buoyant plume above a single heated cylinder presented by Ma and He [17]. At a large vertical pitch (P_v/D=6), however, turbulence initiates right downstream of the bottom cylinder in each column, i.e. at a vertical coordinate of y/D=1.5. Instability originates at the wake downstream of the bottom cylinder, in a pattern that is similar to the wake in flow past a cylinder. Actually, due to the enhancement of natural draft velocity at this vertical pitch, airflow pumped by thermal chimney effect does exert forced convection on the lower and upper cylinders to some degree, although the whole flow field is driven only by buoyancy effect caused by density difference around the heated cylinders.

Accordingly, temperature distribution in the two-row layout also changes substantially when the vertical pitch increases from 4.5D to 6D at the intermediate horizontal pitch of P_h/D=2.5, as shown in Figure 22. At a vertical pitch of 4.5D, the plume is largely laminar and its temperature pattern resembles that around a single horizontal cylinder, as measured by Narayan et al. [26] through laser interferometry. As the vertical pitch increases to 6D, temperature decays rapidly right downstream of the lower and the upper cylinder, due to the initiation of transition to turbulence. Then temperature becomes more diffused transversely due to turbulence dissipation. Thus, preheating effect on the upper cylinder, i.e. immersion of the upper cylinder in the heated plume from the lower cylinder, is weakened.

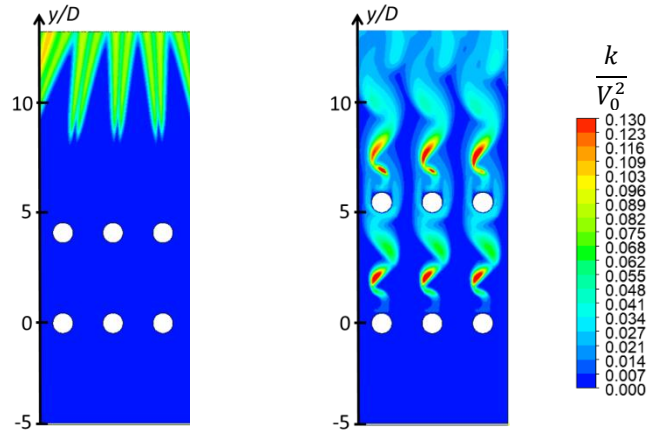

(a) P_v/D=4.5 (b) P_v/D=6

Figure 21. Turbulent kinetic enegy for cylinders in two rows with a horizontal pitch (P_h) of 2.5D at Ra=3.3×10^5 (URANS)

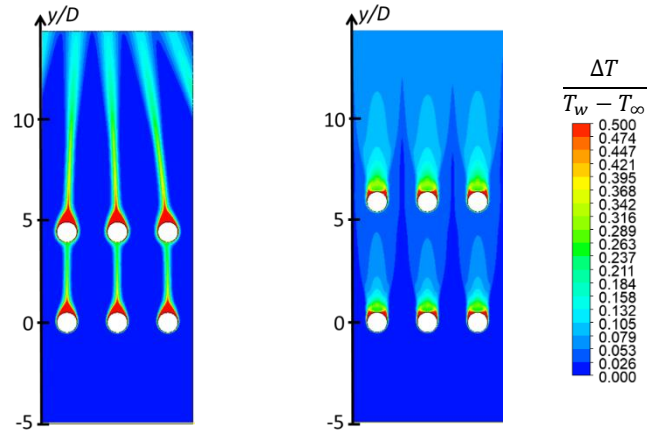

(a) P_v/D=4.5 (b) P_v/D=6

Figure 22. Temperature excess (ΔT) for cylinders in two rows with a horizontal pitch (P_h) of 2.5D at Ra=3.3×10^5 (URANS averaged over 50 s)

Finally, Nusselt number distribution along the circumference of the lower and the upper cylinder with the two vertical pitches (P_v/D=4.5 and 6) at the intermediate horizontal pitch of P_h/D=2.5 is graphed in Figure 23. At the larger vertical pitch of P_v/D=6, Nusselt number along the lower and the upper cylinder surfaces exhibits the same qualitative trend. Nusselt number reduces until a circumferential angle of θ=120°, which is attributed to the thickening of thermal boundary layer along the cylinder surface. It then increases at θ=[120°, 140°], which is probably caused by the flow perturbation of Kelvin-Helmholtz instability between the high velocity jet at the throat of adjacent cylinders (formed by chimney effect) and the low velocity wake behind each cylinder, as manifested in Figure 20b. Nusselt number then decreases and rises again at θ=[150°, 180°], due to the flow perturbations of hot plume leaving each cylinder from trailing edge.

Compared to the smaller vertical pitch of P_v/D=4.5, Nusselt number along the surface of the lower cylinder at the larger vertical pitch (P_v/D=6) increases by up to 20% at θ=[0°, 90°], as a result of the velocity augmentation through the formation of chimney effect, as shown in Figure 20. For the upper cylinder, Nusselt number is higher at the larger vertical pitch (P_v/D=6) for most part of the surface (θ=[20°, 180°]), due to the larger near-wall velocity from chimney effect, as shown in Figure 20. It is only in limited regions near the bottom of the upper cylinder (θ=[0°, 20°]) that the Nusselt number at the smaller vertical pitch (P_v/D=4.5) is higher, because the plume emanating from the lower cylinder impinges on this region directly. Overall speaking, Nusselt number is enhanced at the larger vertical pitch on most part of the cylinder surface, due to the augmentation of upward velocity by chimney effect, which is consistent with the conclusion from Figure 16.

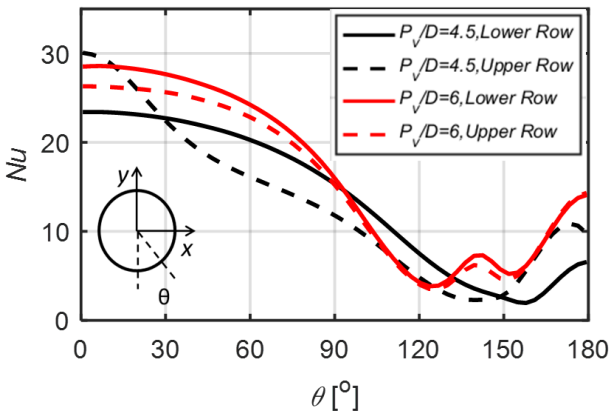

Figure 23. Nusselt number along the circumference of lower (solid curve) and upper (dashed curve) cylinder in two rows with a horizontal pitch (P_h) of 2.5D and a vertical pitch (P_v) of 4.5D (black) and 6D (red) at Ra=3.3×10^5 (URANS averaged over 50 s)

CONCLUSIONS

This paper presents the first of the kind study on natural convection of an array with three or more columns of horizontally-aligned cylinders, to the best of the authors' knowledge. The effects of horizontal and vertical spacings on the natural draft and heat transfer performance of multiple cylinder columns in one or two rows were investigated, through a RANS/URANS approach validated by heat transfer and PIV measurements. RANS with transition SST model is used for preliminary scoping/ranking of thermal chimney designs. URANS is conducted to explore flow physics behind important observations during the parametric study.

For the one-row thermal chimney, an optimum horizontal pitch exists for natural draft velocity, due to the balance between the chimney effect and the blockage effect. The flow field is dominated by buoyant plume downstream of each cylinder at the large horizontal pitch, but by chimney jet at the throat between adjacent cylinders at the small horizontal pitch.

For the two-row thermal chimney, the flow pattern stays plume-dominant at the large horizontal pitch (6D) and chimney-dominant at the small horizontal pitch (2D) for all the eight vertical distances studied. However, at the intermediate horizontal pitch (2.5D), dominant feature of the flow field changes qualitatively from the buoyant plume to the chimney jet as the vertical pitch increases from 4.5D to 6D, leading to prominent augmentation of natural draft velocity and heat transfer on cylinder surfaces. To the authors' knowledge, this unique flow behavior has never been reported in open literature, but is relevant to the design of passive heat exchangers.

ACKNOWLEDGMENTS

The authors would like to thank the financial support from EPSRC Global Challenges Research Fund (EP/P028829/1). The first author would also like to acknowledge funding from

National Natural Science Foundation of China (52106050), Natural Science Foundation of Shanghai (21ZR1431800) and Shanghai Science and Technology Commission Young Talent Sailing Program (20YF1419100). Dr. Sham Rane in University of Oxford is also acknowledged for the valuable discussions.

NOMENCLATURE

Symbols

D	Diameter of cylinder (m)
g	Gravitational constant (=9.8 m^2/s^2)
h	Heat transfer coefficient (W/m^2-K) ($=q''/(T_w - T_\infty)$)
k	Thermal conductivity (W/m-K); Turbulent kinetic energy (m^2/s^2)
Nu	Nusselt number ($=hD/k$)
P	Pressure (Pa)
P_h	Horizontal pitch (m)
P_v	Vertical pitch (m)
q''	Surface heat flux (W/m^2)
Ra	Rayleigh number ($=g\beta\Delta T D^3/\nu\alpha$)
Re_b	Reynolds number at bottom boundary ($=V_{y,b}D/\nu$)
T	Temperature (K)
T_w	Temperature at cylinder surface (K)
T_∞	Ambient temperature (K)
ΔT	Temperature excess (K) ($=T - T_\infty$)
Δt	Time step (s)
V, u	Velocity (m/s)
V_0	Characteristic velocity (m/s)
$V_{y,b}$	Upward velocity at bottom boundary
x	Horizontal coordinate (m)
y	Vertical coordinate (m)

Greeks

α	Thermal diffusivity (m^2/s)
β	Coefficient of thermal expansion (1/K)
ρ	Density (kg/m^3)
ν	Molecular viscosity (m^2/s)
ν_t	Turbulent viscosity (m^2/s)
θ	Circumferential angle (°)

Subscripts

avg	Average
s	Static
t	Total

REFERENCES

[1] Hooman, K., 2015, "Theoretical Prediction With Numerical and Experimental Verification to Predict Crosswind Effects on the Performance of Cooling Towers," Heat Transfer Engineering, 36(5), pp. 480-487.

[2] Lai, K., Wang, W., Yi, C., Kuang, Y., and Ye, C., 2018, "The study of passive cooling system assisted with separate heat pipe for decay heat removal in spent fuel pool," Annals of Nuclear Energy, 111, pp. 523-535.

[3] Zhao, H., Yan, C., Sun, L., Zhao, K., and Fa, D., 2015, "Design of a natural draft air-cooled condenser and its heat transfer characteristics in the passive residual heat removal system for 10 MW molten salt reactor experiment," Applied Thermal Engineering, 76, pp. 423-434.

[4] Wu, X., Yan, C., Meng, Z., Chen, K., Song, S., Yang, Z., and Yu, J., 2016, "Numerical analysis of the passive heat removal system for molten salt reactor at steady state," Applied Thermal Engineering, 102, pp. 1337-1344.

[5] Kröger, D. G., 2004, Air-cooled Heat Exchangers and Cooling Towers: Thermal-flow Performance Evaluation and Design, PennWell Books.

[6] Hooman, K., 2010, "Dry cooling towers as condensers for geothermal power plants," International Communications in Heat and Mass Transfer, 37(9), pp. 1215-1220.

[7] Lu, Y., Guan, Z., Gurgenci, H., Hooman, K., He, S., and Bharathan, D., 2015, "Experimental study of crosswind effects on the performance of small cylindrical natural draft dry cooling towers," Energy Conversion and Management, 91, pp. 238-248.

[8] Kong, Y., Wang, W., Huang, X., Yang, L., Du, X., and Yang, Y., 2018, "Wind leading to improve cooling performance of natural draft air-cooled condenser," Applied Thermal Engineering, 136, pp. 63-83.

[9] Tanimizu, K., and Hooman, K., 2013, "Natural draft dry cooling tower modelling," Heat and Mass Transfer, 49(2), pp. 155-161.

[10] Zou, Z., Guan, Z., Gurgenci, H., and Lu, Y., 2012, "Solar enhanced natural draft dry cooling tower for geothermal power applications," Solar Energy, 86(9), pp. 2686-2694.

[11] Zou, Z., Guan, Z., and Gurgenci, H., 2013, "Optimization design of solar enhanced natural draft dry cooling tower," Energy Conversion and Management, 76, pp. 945-955.

[12] Ghorbani, B., Ghashami, M., and Ashjaee, M., 2015, "Electricity production with low grade heat in thermal power plants by design improvement of a hybrid dry cooling tower and a solar chimney concept," Energy Conversion and Management, 94, pp. 1-11.

[13] Morgan, V. T., 1975, "The Overall Convective Heat Transfer From Smooth Circular Cylinders," Advances in Heat Transfer, Elsevier, pp. 199-264.

[14] Churchill, S. W., and Chu, H. H., 1975, "Correlating Equations for Laminar and Turbulent Free Convection from a Horizontal Cylinder," International Journal of Heat and Mass Transfer, 18(9), pp. 1049-1053.

[15] Atayılmaz, Ş. Ö., and Teke, İ., 2009, "Experimental and Numerical Study of the Natural Convection from a Heated Horizontal Cylinder," International Communications in Heat and Mass Transfer, 36(7), pp. 731-738.
[16] Kitamura, K., Kami-Iwa, F., and Misumi, T., 1999, "Heat transfer and fluid flow of natural convection around large horizontal cylinders," International Journal of Heat and Mass Transfer, 42(22), pp. 4093-4106.
[17] Ma, H., and He, L., 2021, "Large eddy simulation of natural convection heat transfer and fluid flow around a horizontal cylinder," International Journal of Thermal Sciences, 162.
[18] Chae, M.-S., and Chung, B.-J., 2011, "Effect of pitch-to-diameter ratio on the natural convection heat transfer of two vertically aligned horizontal cylinders," Chemical Engineering Science, 66(21), pp. 5321-5329.
[19] Sparrow, E., and Niethammer, J., 1981, "Effect of vertical separation distance and cylinder-to-cylinder temperature imbalance on natural convection for a pair of horizontal cylinders," Journal of Heat Transfer, 103(4), pp. 638-644.
[20] Heo, J.-H., Chae, M.-S., and Chung, B.-J., 2013, "Influences of vertical and horizontal pitches on the natural convection of two staggered cylinders," International Journal of Heat and Mass Transfer, 57(1), pp. 1-8.
[21] Stafford, J., and Egan, V., 2014, "Configurations for single-scale cylinder pairs in natural convection," International Journal of Thermal Sciences, 84, pp. 62-74.
[22] Persoons, T., O'Gorman, I. M., Donoghue, D. B., Byrne, G., and Murray, D. B., 2011, "Natural convection heat transfer and fluid dynamics for a pair of vertically aligned isothermal horizontal cylinders," International Journal of Heat and Mass Transfer, 54(25-26), pp. 5163-5172.
[23] Corcione, M., 2005, "Correlating equations for free convection heat transfer from horizontal isothermal cylinders set in a vertical array," International Journal of Heat and Mass Transfer, 48(17), pp. 3660-3673.
[24] Kitamura, K., Mitsuishi, A., Suzuki, T., and Kimura, F., 2016, "Fluid flow and heat transfer of natural convection induced around a vertical row of heated horizontal cylinders," International Journal of Heat and Mass Transfer, 92, pp. 414-429.
[25] Corcione, M., 2007, "Interactive free convection from a pair of vertical tube-arrays at moderate Rayleigh numbers," International journal of heat and mass transfer, 50(5-6), pp. 1061-1074.
[26] Narayan, S., Singh, A. K., and Srivastava, A., 2017, "Interferometric study of natural convection heat transfer phenomena around array of heated cylinders," International Journal of Heat and Mass Transfer, 109, pp. 278-292.
[27] Park, Y. G., Ha, M. Y., and Park, J., 2015, "Natural convection in a square enclosure with four circular cylinders positioned at different rectangular locations," International Journal of Heat and Mass Transfer, 81, pp. 490-511.
[28] Chen, H.-T., Ma, W.-X., and Lin, P.-Y., 2020, "Natural convection of plate finned tube heat exchangers with two horizontal tubes in a chimney: Experimental and numerical study," International Journal of Heat and Mass Transfer, 147.
[29] Briggs, D. E. Y., Edwin H. , 1963, "Convection heat transfer and pressure drop of air flowing across triangular pitch banks of finned tubes," Chem. Eng. Prog. Symp. Ser.
[30] Gyles, B. R., Hægland, B., Dahl, T. B., Sanchis, A., Grafsrønningen, S., and Jensen, A., 2011, "Natural convection-subsea cooling: theory, simulations, experiments and design," ASME 2011 30th International Conference on Ocean, Offshore and Arctic EngineeringRotterdam, Netherlands, pp. 11-20.
[31] Li, W., Yu, G., Zagaglia, D., Green, R., and Yu, Z., 2020, "CFD modelling of a thermal chimney for air-cooled condenser," Geothermics, 88.
[32] Ma, H., He, L., and Rane, S., "Heat Transfer-Fluid Flow Interaction in Natural Convection around Heated Cylinder and Its Thermal Chimney Effect," Proc. International Conference on Innovative Applied Energy.
[33] Yu, G., Zagaglia, D., Green, R., and Yu, Z., 2020, "Particle Image Velocimetry (PIV) experiment of the buoyant flow field of a thermal chimney model designed for geothermal power plants," International Journal of Green Energy, 17(15), pp. 951-960.
[34] Coleman, H. W., and Steele, W. G., 2009, Experimentation, Validation, and Uncertainty Analysis for Engineers, John Wiley & Sons.
[35] Webb, A., and Mansour, N., 2000, "Towards LES models of jets and plumes," Center for Turbulence Research, Annual Research Briefs, 2000, pp. 229-240.
[36] Grafsrønningen, S., and Jensen, A., 2017, "Large eddy simulations of a buoyant plume above a heated horizontal cylinder at intermediate Rayleigh numbers," International Journal of Thermal Sciences, 112, pp. 104-117.
[37] Pope, S. B., 2001, "Turbulent flows," IOP Publishing.
[38] Menter, F. R., Langtry, R. B., Likki, S. R., Suzen, Y. B., Huang, P. G., and Volker, S., 2006, "A correlation-based transition model using local variables - Part I: Model formulation," Journal of Turbomachinery, 128(3), pp. 413-422.
[39] Grafsrønningen, S., Jensen, A., and Reif, B. A. P., 2011, "PIV investigation of buoyant plume from natural convection heat transfer above a horizontal heated cylinder," International Journal of Heat and Mass Transfer, 54(23-24), pp. 4975-4987.
[40] Kuehner, J. P., Hamed, A., and Mitchell, J. D., 2015, "Experimental investigation of the free convection velocity boundary layer and plume formation region for a heated horizontal cylinder," International Journal of Heat and Mass Transfer, 82, pp. 78-97.
[41] Pelletier, Q., Murray, D. B., and Persoons, T., 2016, "Unsteady natural convection heat transfer from a pair of vertically aligned horizontal cylinders," International Journal of Heat and Mass Transfer, 95, pp. 693-708.
[42] Chen, H.-T., Lin, Y.-S., Chen, P.-C., and Chang, J.-R., 2016, "Numerical and experimental study of natural convection heat transfer characteristics for vertical plate fin and tube heat exchangers with various tube diameters," International Journal of Heat and Mass Transfer, 100, pp. 320-331.

[43] Sebastian, G., and Shine, S., 2015, "Natural convection from horizontal heated cylinder with and without horizontal confinement," International Journal of Heat and Mass Transfer, 82, pp. 325-334.